# Coordination Control of a Dual-arm Exoskeleton Robot Using Human Impedance Transfer Skills

Bo Huang, Zhijun Li, Xinyu Wu, Arash Ajoudani, Antonio Bicchi, and Junqiang Liu

***Abstract*—This paper develops a coordination control method for a dual-arm exoskeleton robot based on human impedance transfer skills, where the left (master) robot arm extracts the human limb impedance stiffness and position profiles, and then transfers the information to the right (slave) arm of the exoskeleton. A computationally efficient model of the arm endpoint stiffness behavior is developed and a co-contraction index is defined using muscular activities of a dominant antagonistic muscle pair. A reference command consisting of the stiffness and position profiles of the operator is computed and realized by one robot in real-time. Considering the dynamics uncertainties of the robotic exoskeleton, an adaptive-robust impedance controller in task space is proposed to drive the slave arm tracking the desired trajectories with convergent errors. To verify the robustness of the developed approach, a study of combining adaptive control and human impedance transfer control under the presence of unknown interactive forces is conducted. The experimental results of this paper suggest that the proposed control method enables the subjects to execute a coordination control task on a dual-arm exoskeleton robot by transferring the stiffness from the human arm to the slave robot arm, which turns out to be effective.***

***Index Terms*—Impedance control, biomimetic, stiffness estimation, adaptive robust control, coordination control.**

## I. Introduction

Assistive robot exoskeletons can provide motion support to humans, especially be applicable to the elder or the patients with impaired muscles that are not able to generate necessary amount of forces to perform intended tasks [1], [2], [3]. On the other hand, robotic exoskeletons are also used to strengthen the power of healthy people and enhance their endurance for heavy tasks. It has been verified that humans can interact with changeable environments with steady and applicable skills, which can be accomplished by the adjustment of the mechanical properties of the upper limbs [4]. In some efforts on dealing with the weakness of traditional tele-operation interfaces, the concept of tele-impedance control has been recently presented [5], [6]. Several related interaction works verified the effectiveness of the control concepts [7], [8]. To establish a novel human machine interface, the motion trajectories and impedance information are achieved by the left (master) arm of the exoskeleton robot from the wearing human body in real-time. Then the right (slave) arm of the exoskeleton receives the relevant profiles and performs the corresponding manipulation.

Neuromotor experimental studies have shown that the impedance of human joints can be voluntarily adapted during motion tasks. If delicate impedance adaptation skills of the human operator can be incorporated into the robot control, it would greatly benefit the physical human-robot interaction [9]. It is well known that the limb endpoint visco-elastic properties can be regulated by relevant muscles and pose configurations in different ways. In [10], the regulation can be achieved by co-contracting muscles acting on the limb, and it can be acquired as well through the adaptation in the sensitivity of the reflex feedback [11], or the selective control of limb configurations [12]. In [13], [14], a position perturbation was implemented to the hand, and the related forces and displacements were acquired and recorded by the specified device. Then, the impedance parameters were estimated by undergoing a post-processing stage. In [15], the estimation of dynamic impedance profiles using perturbation based methods in multi-joint arm movements has been widely studied. However, perturbation based approaches are hard to implement in the real-time manipulation, for the intrusion of the external disturbances. Consequently, some suitable human machine interfaces have been investigated for real-time applications [5], [16], [17].

It is well known that surface electromyography (sEMG) signals have close relationships with muscle activations, muscular forces and joint torque profiles. Therefore, sEMG signals are widely used to capture the real-time joint/endpoint stiffness profiles. In [18], a straightforward model which assumes a linear relationship between the end-point stiffness and rectified sEMG signals was applied in the fixed posture configuration. In this linear model, a complex modelling of the muscular-skeletal system seems to be necessary when estimating the whole arm workspace stiffness [16]. However, related researches on human motor behaviors presented that this complexity can be solved by the central nervous system (CNS) in an efficient way [19], [20].

Relevant observations about human neuromotor control of the human arm endpoint stiffness found out that for realizing a required endpoint stiffness direction, humans gravitate towards maximize the use of limb postures [5], [21]. The configuration-dependent properties of the joint and Cartesian stiffness were explored and a reduced-complexity model of arm endpoint stiffness was established in [22].

Considering that there are large external disturbances on the human limb, the human will naturally make his muscles tight so the impedance of his body will increase to compensate for the disturbances. While the disturbances decrease, impedance will be reduced and muscles are in relax. Considering how humans can skilfully adapt impedance in various force inter-

B. Huang, Z. Li and J. Liu are currently with The Key Lab of Autonomous System and Network Control, College of Automation Science and Engineering, South China University of Technology, Guangzhou, China, Email:zjli@ieee.org.

X. Wu is with Shenzhen Institutes of Advanced Technology, Chinese Academy of Sciences, 1068 Xueyuan Ave, Shenzhen, Guangdong, China. Email: xy.wu@siat.ac.cn.

A. Ajoudani, and A. Bicchi are with the Dept. of Advanced Robotics, Istituto Italiano di Tecnologia, Via Morego 30, 16163, Genova, Italy. Arash Ajoudani and A. Bicchi are also with Interdepartmental Research Center "E. Piaggio", Faculty of Engineering, University of Pisa, Italy. e-mails: arash.ajoudani@iit.it, and bicchi@centropiaggio.unipi.it.

active scenarios, we would like to transfer this flexibility to the robot to compensate the disturbances. One possibility to adapt the impedance is by using human-like adaptation. The human-like adaptive method transfers the adaptive impedance skill to the robot, which instead of automatic learning, extracts impedance adaptation skills and then implements on the robot to imitate humans compliance and adaptivity. Nowadays, in the rehabilitation area, for reducing the workloads of the physical therapist, the researchers have paid attentions to exoskeleton robots. And our work is motivated by the previous studies in this area. We proposed a method which transfers the human stiffness and position profiles to the exoskeleton which could follow the motions of the human with human-like skills. And this method has great room for the development of the rehabilitation area.

Impedance transferred by the human can be used as control signals for the robot manipulation. However, it may be delicate to achieve desirable performances in the sophisticated environment with perturbations only relying on the impedance adaptation. To make a good performance on disturbance rejections and to achieve small tracking errors, it is necessary to utilize the relevant robot automatic control. Recently, there are some works conducted to investigate the disturbance observer techniques in motion control [23], [24], [25], [26]. Disturbance observer-based control with a simple structure can be used to compensate for various uncertainties, but it cannot adequately compensate all the uncertainties if there exists uncertain dynamics and fast varying perturbations.

In order to overcome the dynamics uncertainties, adaptive control methods can be alternated [27], [28], [29]. Adaptive control laws would attain an accurate tracking of the required trajectories in the case that the external disturbances can be parameterized. On the other hand, the adaptive laws may not perform well when encountering unparameterizable uncertainties through the adaptation process. In [30], [31], disturbance observer based control and reinforcement learning are utilized to approximate the uncertain dynamics and resist the time-varying disturbances.

In this paper, a control framework which combines the human stiffness transfer control and the adaptive control is established. In [34], [35], [36], the combination of the human stiffness transfer and the adaptive control is also investigated. With the haptic communication with the environment, the human operator perceives forces and transfers the adaptive impedance to the robot. In contrast to the above works, we investigated this specific area in a different way. Based on the relevant research [22] on the profile between the sEMG signals and the end-point stiffness, we utilized the sEMG signals to transfer the human stiffness to the controller of the exoskeleton. In addition, the adaptive control law also participates in the control framework to get better performances on rejecting the external disturbances in the dynamic movement. We verified the effectiveness of our method through specific experiments on a dual-arm exoskeleton robot platform.

In this paper, we followed the standard methods of identifying human arm end-point stiffness in Cartesian space [14], and applied the stochastic disturbances to the end point of the slave robot. The external forces were collected by a force sensor SRI-M3203 (Sunrise Instrument Co., Ltd), which was placed at the endpoint of the slave arm of the exoskeleton robot. The operator wears the exoskeleton robot and the motors of the robot can record the real-time angles of the master robot for the calculation of the Jacobian matrix. The sEMG signal collector records the real-time signals of the related muscles. These relevant equipments are shown in Fig. 1.

The contributions of this paper are as follow:

(1) An approach of coordination control of a dual-arm exoskeleton robot is developed based on human impedance transfer skills, where the human stiffness and position profiles are transferred to the slave robot arm.

(2) The reference command consisting of the stiffness and position profiles is computed and realized in real-time.

(3) An adaptive-robust impedance controller in task space is developed to drive the slave arm of the exoskeleton tracking the desired trajectories with convergent errors when the perturbations exist.

## II. Cartesian Stiffness Modelling of Human Arm

### A. Conservative Stiffness Matrix

The congruence transformation with the stiffness matrices between Cartesian space and joint space is usually a nonconservative mapping [37]. The transformation is given by

$$K_J(q) = J_r^T(q) K_c(q) J_r(q) \tag{1}$$

with the joint stiffness matrices $K_J(q)$, the Cartesian stiffness matrices $K_c(q)$, the joint angle vector $q$, and the matrix $J_r(q) \in \mathbb{R}^{m\times n}$ which is assumed to be nonsingular in the finite work space $\Omega$ is the manipulator Jacobian with $n$ being the number of joints of the human limb and $m$ corresponding to the task space dimensions.

The inverse transform can be described as follow [38]:

$$K_c(q) = (J_r^+(q))^T K_J(q) (J_r(q))^+ \tag{2}$$

where $J_r^+(q)$ is the generalized inverse matrix of $J_r(q)$.

Fig. 2 demonstrates the congruence transformation between the joint stiffness matrix and Cartesian stiffness matrix and its inverse mapping. The Jacobian matrix with the differential parameters in the joint and Cartesian spaces is usually configuration-dependent. The matrix $J_r$ would change as the specified movements are carried out, which leads to the stiffness matrix to be configuration-dependent.

In Fig. 2, the Cartesian stiffness $D_1$ is expressed in an $m$ dimensions space. When the congruence mapping (1) is performed, the corresponding joint stiffness $C_1$ can be obtained in the joint space and is expressed in $n$ angles in the n-DOF robot arm.

### B. The Cartesian Stiffness Modelling of Human Arm

Humans are able to interact with the changeable environments with steady and applicable skills, which can be accomplished by the adjustment of the mechanical properties of the upper limbs [4]. Therefore, extracting impedance adaptation skills from the human operator and incorporating it into the robot control would be an economic method for


Fig. 1. The relevant equipments of the endpoint stiffness estimation: i) The upper limb exoskeleton robot; ii) The force sensor SRI-M3203 (equipped at the end point of the slave robot arm to measure the perturbations); iii) The sEMG signal collector.

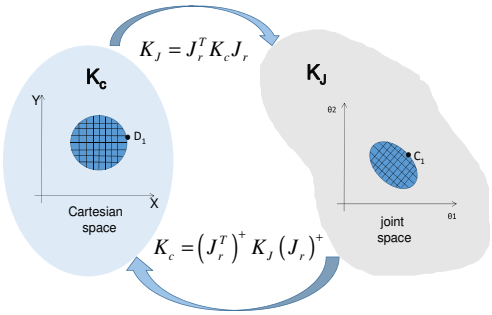


Fig. 2. The congruence mapping.

the human-robot interaction [9]. Generally speaking, the end-point stiffness of the human upper limb is effected by the relevant muscle groups and the pose configuration adjustments. It implies that we are able to adopt the end-point stiffness by contracting of relevant muscle groups as well as the pose configuration adjustments.

According to the studies in neuromotor control of human arm end-point stiffness, humans are likely to fully exploit the use of limb postures to grasp a related end-point stiffness direction [21], [22]. Therefore, in some specific applications, the configuration-dependent effect of the joint stiffness matrix can be neglected. Based on this consideration, the active joint stiffness regulations $K_J$ can be modeled as follow [22]:

$$K_J = a_{cc}\bar{K}_J \tag{3}$$

where $\bar{K}_J$ represents the joint stiffness matrix of minimum muscle activity, and $a_{cc}$ a size-adjusting co-contraction index. Index $a_{cc}$ is influenced by the muscular activities which are realized by the sEMG signals of the dominant antagonistic muscle pair. The end-point stiffness of the human arm in Cartesian space $K_c$ can be represented as follow [22]:

$$K_c(q) = (J_r^+(q))^T \left[a_{cc}\bar{K}_J - Z_J(q)\right](J_r(q))^+ \tag{4}$$

$$Z_J(q) = \frac{\partial \tau_g(q)}{\partial q} \tag{5}$$

where $K_c \in \mathbb{R}^{m\times n}$, $n$ denotes the number of joints of the human limb, $m$ denotes the task space dimensions and $m = n$ is assumed in this paper. $q \in \mathbb{R}^n$ is a vector of $n$ joint angles of the arm. $J_r(q)$ is the Jacobian matrix of the human arm, and $Z_J(q)$ defines the effect of gravity $\tau_g(q)$ on Cartesian stiffness. In order to get the precise performances of relevant posture configurations, a novel way of obtaining the Jacobian matrix is implemented in our work [22]. In detail, the operator is required to wear the master arm of the exoskeleton robot to obtain the Jacobian and transfer it to the controller in real-time.

In addition, A compact model in estimating the human arm gravitational torque is used in this paper [22], [39]. The definition is shown as follow:

$$\tau_g(q) = \sum_{i=1}^{n_J} J_{com_i}^T(q) m_i \mathbf{g} \tag{6}$$

where $J_{com_i}, m_i, n_J$ and $\mathbf{g}$ indicate the centre of mass Jacobian, the mass of the $i$th limb, the joint number, and the gravitational vector, respectively.

## III. Human Arm Endpoint Stiffness Estimation

To estimate the end-point stiffness of the human arm in (4), we firstly need to acquire $a_{cc}, \bar{K}_J, J_r(q), Z_J$. Just as mentioned before, the Jacobian matrix can be obtained by the exoskeleton robot in real-time, and the structure of the exoskeleton robot arm is represented in Fig. 3. As a result, to obtain the other two parameters is the major portion. Since that muscular activations are highly related to the active joint stiffness [17], and that muscular activations can be reflected from sEMG signals, we achieved and processed the sEMG signals of related muscles by using specific tools.

The target end-point stiffness $K_c$ is suggested to use in the dynamic movements of the human limb. In this direction, it is necessary to identify $K_c$ in different posture configurations and different co-contraction amplitudes of relevant muscle groups. In this experiment, three different co-contractions of muscle groups are taken into consideration. The measurement of the three co-contractions is to obtain the sEMG signals while the operator is contracting his muscles and applying the forces of 4 N, 8 N and 12 N. The operator is asked to exert such three different forces along 6 directions $[\pm X, \pm Y, \pm Z]$ on the force sensor. Meanwhile, the force data is shown for the operator to maintain the forces with visual feedback. In detail, the minimum-activity group is used to estimate the parameter $\bar{K}_J$, and the other two groups are used to estimate of the index $a_{cc}$.

Six different positions are implemented in the experiments. There are two indicators when choosing these configurations: the comfort of the operator and the avoidance of the singularity of the Jacobian matrix. In each position, arm joints were

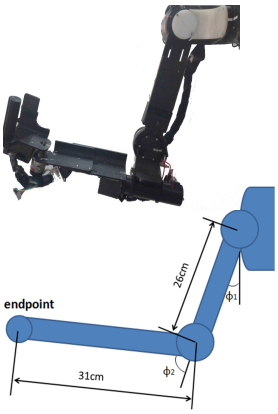


Fig. 3. The structure of the exoskeleton robot arm.

allowed to vary within the redundant manifold to realize three distinct angles of the related joint. It would be 18 arm configurations. Furthermore, in each configuration, three different co-contractions of muscle groups were required: minimum-activity, middle-activity and high-activity. As a result, it would have 54 groups of data for estimating the end-point stiffness.

During the experiment, sEMG data from relevant muscles (Biceps and Triceps Brachii) was obtained by using surface electrodes (as is shown in Fig. 1) which are connected to the sEMG signal collector. In signal processing stages, a bandpass filter and a notch filter are used. The relative parameters in the bandpass filter are chosen as 10 and 500 Hz and the parameter in the notch filter is chosen as 50 Hz. All the filters were realized by employing Butterworth filtering technique.

After collecting the experimental data, the next step is to identify $a_{cc}, \bar{K}_J$ from these data. A dynamic relation between the displacements and forces is shown as follow [22], [40]:

$$\begin{bmatrix} F_x(f) \\ F_y(f) \\ F_z(f) \end{bmatrix} = \begin{bmatrix} N_{xx}(f) & N_{xy}(f) & N_{xz}(f) \\ N_{yx}(f) & N_{yy}(f) & N_{yz}(f) \\ N_{zx}(f) & N_{zy}(f) & N_{zz}(f) \end{bmatrix} \begin{bmatrix} x(f) \\ y(f) \\ z(f) \end{bmatrix} \quad (7)$$

where $F_x(f)$, $F_y(f)$ and $F_z(f)$ denote the Fourier transforms of the endpoint forces along the axes of the Cartesian reference frame; $x(f)$, $y(f)$ and $z(f)$ denote the Fourier transforms of the human endpoint displacements; $N_{ij}$ denotes the second-order, linear model of each impedance transfer function of each SISO (single input and single out) subsystem:

$$N_{ij}(s) = I_{ij}s^2 + V_{ij}s + K_{ij}, \quad s = 2\pi f\sqrt{-1} \quad (8)$$

where $I_{ij}$, $V_{ij}$ and $K_{ij}$ denote the endpoint inertia matrix, the endpoint viscosity matrix and the endpoint stiffness matrix, respectively.

In the post-processing phase, the stiffness matrices from the minimum activity groups were utilized to calculate $\bar{K}_J$ by minimizing

$$\left\| \bar{K}_J - J_r^T(q) K_c J_r(q) - \frac{\partial \tau_g(q)}{\partial q} \right\| \quad (9)$$

In addition, we obtained the index $a_{cc}$ with analyzing the data of the mid and the high co-contractions of muscle groups. A hyperbolic tangent function is employed to denote $a_{cc}$ [8], [41] :

$$a_{cc} = 1 + \frac{r_1[1 - e^{-r_2(M_B + M_T)}]}{[1 + e^{-r_2(M_B + M_T)}]} \quad (10)$$

where $M_B$ and $M_T$ indicate the real-time sEMG signals of Biceps and Triceps Brachii muscles, and $r_1$ and $r_2$ are constant coefficients that can be identified by minimizing

$$\left\| a_{cc}(p)\bar{K}_J - J_r^T(q) K_c J_r(q) - \frac{\partial \tau_g(q)}{\partial q} \right\| \quad (11)$$

## IV. Dual-arm Exoskeleton System Description

A dual arm exoskeleton robot consisting of two 4-DOF exoskeleton platforms has been developed for the experiments in SCUT lab, as shown in Fig. 4. Each arm has 4 joints, such as shoulder abduction/adduction joint, shoulder rotation joint, elbow joint, wrist joint. The shoulder rotation joint and elbow joint of the exoskeleton are used in the experiments. The kinematical chain is similar to the upper limb of a human being. In the developed exoskeleton, each joint contains a high-resolution encoder (2048 pulse/cycle) and a hall effect sensor used for position sensing and measurements. The robotic exoskeleton is developed using DC motors as actuators, and Maxon DC flat brushless motor EC45 is chosen as the driver unit. To get a better performance of the impedance capability, each joint of the robot have been embedded a harmonic transmission driver.

The subject wears one exoskeleton arm and controls the trajectories of the moving arm as the master and the other exoskeleton arm performs as the slave. Meanwhile, sEMG signals are acquired from Biceps and Triceps Brachii muscles of the subject. The master exoskeleton robot collects the real-time tracking of the human arm kinematics and calculates the real-time human arm Jacobian. While the human arm Jacobian and the sEMG signals are transferred to the controller, the endpoint stiffness can be calculated by the muscular co-activations and trajectories.

## V. Control Development of Slave Exoskeleton

The dynamics of the robotic exoskeleton in joint space can be described by

$$M(q)\ddot{q} + C(q,\dot{q})\dot{q} + G(q) + d = B(q)\tau \quad (12)$$

with $q = [q_1, \ldots, q_n]^T \in R^n$, the symmetric positive definite inertia matrix $M(q) \in R^{n\times n}$ , the Centripetal and Coriolis torques $C(\dot{q}, q) \in R^{n\times n}$ , the gravitational torque vector $G(q) \in R^n$ , the external disturbances $d(t) \in R^n$, and the control inputs $\tau \in R^k$, and a full rank known input transformation matrix $B(q) \in R^{n\times k}$ for the robotic manipulator.

The equation of motion of the manipulator could be rewritten in terms of Cartesian coordinates $x \in R^n$. We assume

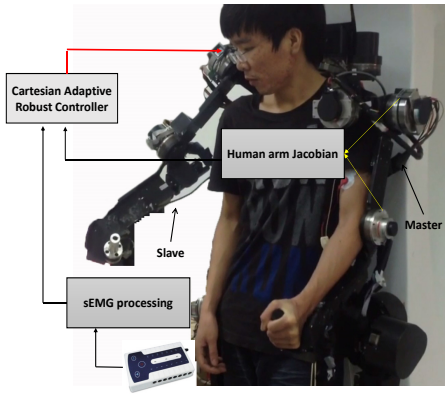


Fig. 4. The developed dual-arm exoskeleton.

that the relationship between the Cartesian coordinates and the joint coordinates is shown as follows:

$$\dot{x} = J_r \dot{q} \tag{13}$$

where $J_r \in R^{n\times n}$ is the Jacobian matrix. Considering the differential of (13) with respect to time, we obtain

$$\ddot{x} = J_r \ddot{q} + \dot{J}_r \dot{q} \tag{14}$$

Since we assume that Jacobian matrix $J_r$ is nonsingular

$$\ddot{q} = J_r^{-1}(\ddot{x} - \dot{J}_r \dot{q}) \tag{15}$$

Integrating (13), (15) into (12), we can obtain

$$\mathcal{M}\ddot{x} + \mathcal{C}\dot{x} + \mathcal{G} + \mathcal{D} = \mathcal{U} \tag{16}$$

where

$$\begin{aligned} \mathcal{M} &= J_r^{+T} M(q) J_r^{+} \\ \mathcal{C} &= J_r^{+T}(-M(q)J_r^{-}\dot{J}_r + C(q,\dot{q}))J_r^{+} \\ \mathcal{G} &= J_r^{+T} G(q) \\ \mathcal{D} &= J_r^{+T} d \\ \mathcal{U} &= J_r^{+T} B(q)\tau \end{aligned}$$

To make a better control performance, we consider an impedance model with virtual force as follow

$$M_d\ddot{x}_d + C_d\dot{x}_d + K_c x_d = f \tag{17}$$

where $M_d$ and $C_d$ are the desired inertia, damping,respectively, and $K_c$ represents the Cartesian stiffness of the endpoint of manipulator and it is calculated by (4) in section II, and $f$ can be regarded as a virtual force.

There are some structure properties of the dynamic equation (16), which will become useful when designing the specific control system.

*Property 5.1:* [42] There exists the bounded symmetric positive definite matrix $\mathcal{M}$, i.e., $\lambda_{min}(\mathcal{M})I \le \mathcal{M} \le \lambda_{max}(\mathcal{M})I$, with the minimum eigenvalues $\lambda_{min}(\mathcal{M})$ and maximum eigenvalues $\lambda_{max}(\mathcal{M})$ of $\mathcal{M}$.

*Property 5.2:* [42] The skew-symmetric matrix $\dot{\mathcal{M}} - 2\mathcal{C}$ satifies $\forall u \in R^n$, $u^T(\dot{\mathcal{M}} - 2\mathcal{C})u = 0$.

*Property 5.3:* There exist inequalities $\forall x \in R^n$, $\forall \dot{x} \in R^n$, $||\mathcal{M} + M_d|| \le c_1$, $||\mathcal{C} + C_d|| \le c_2 + c_3||\dot{q}||$, $||\mathcal{G}|| \le c_4$ , $||M_d|| \le c_5$ and $||C_d|| \le c_6$, $\sup_{t\ge 0}||\mathcal{D}|| \le c_7$, with the finite positive constants $c_k > 0$ $(1 \le k \le 6)$, and a finite non-negative constant $c_k \ge 0$ $(k = 7)$.

Considering a desired motion trajectory $x_d(t)$, which is bounded and uniformly continuous and has bounded and uniformly continuous derivatives up to the third order, we need to design a control law such that for any $(x(0), \dot{x}(0)) \in \Omega$, $(x, \dot{x})$ converge to a manifold specified as $\Omega$ where

$$\Omega_d = \{(x,\dot{x}) | x = x_d, \dot{x} = \dot{x}_d\} \tag{18}$$

*Definition 5.1:* Consider a time varying positive function $\delta$, which will converges to 0 as $t \to \infty$ and be bounded by

$$\lim_{t\to\infty} \int_0^t \delta(\omega) d\omega = \rho < \infty$$

where $\rho$ is a finite constant [43].

In the actual implementation, we choose $\delta = 1/(1+t)^2$ in the experiment.

Let $e = x - x_d$, $\dot{x}_r = \dot{x}_d - \varpi e$, $s = \dot{e} + \varpi e$, where $\varpi$ is diagonal positive definite. Based on (16), we consider the robust adaptive control law given by

$$\begin{aligned} \mathcal{U} &= -K_m s - \sum_{i=1}^{7} \frac{s\hat{c}_i \Phi_i^2}{\|s\|\Phi_i + \delta_i} - f \\ \dot{\hat{c}}_i &= -\sigma_i \hat{c}_i + \frac{\gamma_i \Phi_i^2 \|s\|^2}{\Phi_i \|s\| + \delta_i} \end{aligned} \tag{19}$$

where $K_m$ is a suitable definite constant; $\Phi_1 = \|\ddot{x}_r\|$, $\Phi_2 = \|\dot{x}_r\|$, $\Phi_3 = \|\dot{q}\|\|\dot{x}_r\|$, $\Phi_4 = 1$, $\Phi_5 = \|\dot{e}\|$, $\Phi_6 = \|e\|$ and $\Phi_7 = 1$; $\gamma_i > 0$, $\delta_i(t) > 0$ and $\sigma_i(t) > 0$ such that $\int_0^t \delta_i(\omega)d\omega = a_i < \infty$ and $\int_0^t \sigma_i(\omega)d\omega = b_i < \infty$.

The external force exerted at the end point of the slave arm can be viewed as a perturbation in the robotic dynamics. The control (19) is designed to make the slave track the desired trajectory and reject the perturbation.

Compared with the previous results [22], in the proposed robust adaptive control (19), the second item of the controller is designed to approximate the dynamics uncertainties, where $\hat{c}_i$ is the estimation of the upper bound of the adaptive parameter $c_i$. The item $f$ is designed to reject the perturbation by the transferred impedance. Compared with the previous results [24] which did not consider the impedance model, in the paper, the combination of the impedance model (17) and the adaptive control (19) can approximate the uncertain dynamics.

*Theorem 5.1:* Consider the robotic exoskeleton described by (16), by the control law (19), the following holds for any $(x(0), \dot{x}(0)) \in \Omega$:

i) $s$ would converge to a set that containing the origin and the convergence rate could represent as $e^{-\nu t}$.

ii) $e$ and $\dot{e}$ asymptotically converge to zero as $t \to \infty$.

*Proof*: i). By taking (19) into (16), we can obtain the following closed-loop system as

$$\mathcal{M}\dot{s} = -K_m s - \sum_{i=1}^{7} \frac{s\hat{c}_i \Phi_i^2}{\|s\|\Phi_i + \delta_i} - \xi - K_c x_d - \mathcal{C}s \tag{20}$$

where $\xi = (M_d+\mathcal{M})\ddot{x}_r+(C_d+\mathcal{C})\dot{x}_r+\mathcal{G}+\mathcal{D}+M_d\varpi\dot{e}+C_d\varpi e$.

Consider the Lyapunov candidate function with $\tilde{c}_i = \hat{c}_i - c_i$:

$$V = \frac{1}{2}s^T\mathcal{M}s + \sum_{i=1}^{7}\frac{1}{2\gamma_i}\tilde{c}_i^2 \tag{21}$$

then

$$\dot{V} = s^T(\mathcal{M}\dot{s} + \frac{1}{2}\dot{\mathcal{M}}s) + \sum_{i=1}^{7}\frac{\tilde{c}_i\dot{\tilde{c}}_i}{\gamma_i} \tag{22}$$

From Property 5.1, we have $\frac{1}{2}\lambda_{min}(\mathcal{M})s^Ts \leq V \leq \frac{1}{2}\lambda_{max}(\mathcal{M})s^Ts + \Lambda$, where $\Lambda$ is a positive constant. By using Property 5.2, the time derivative of $V$ along the trajectory of (20) is

$$\begin{aligned}
\dot{V} &= -s^TK_ms - \sum_{i=1}^{7}\frac{\|s\|^2\hat{c}_i\Phi_i^2}{\|s\|\Phi_i+\delta_i} + \sum_{i=1}^{7}\frac{\tilde{c}_i\dot{\tilde{c}}_i}{\gamma_i} \\
&\quad -s^TK_cx_d - s^T\xi \\
&\leq -s^TK_ms - s^TK_cx_d + \sum_{i=1}^{7}\|s\|c_i\Phi_i - \sum_{i=1}^{7}\frac{\|s\|^2\hat{c}_i\Phi_i^2}{\|s\|\Phi_i+\delta_i} \\
&\quad + \sum_{i=1}^{7}\tilde{c}_i(-\frac{\sigma_i}{\gamma_i}\hat{c}_i + \frac{\Phi_i^2\|s\|^2}{\Phi_i\|s\|+\delta_i}) \\
&\leq -s^TK_ms + \frac{\|K_c\|}{2}(\|s\|^2+\|x_d\|^2) + \sum_{i=1}^{7}(\|s\|c_i\Phi_i \\
&\quad - \frac{\|s\|^2\hat{c}_i\Phi_i^2}{\|s\|\Phi_i+\delta_i} - \frac{\sigma_i}{\gamma_i}\hat{c}_i\tilde{c}_i + \frac{\Phi_i^2\|s\|^2(-c_i+\hat{c}_i)}{\Phi_i\|s\|+\delta_i}) \\
&\leq -s^T(K_m - \frac{\|K_c\|}{2})s + \frac{\|K_c\|\|x_d\|^2}{2} \\
&\quad + \sum_{i=1}^{7}\frac{\Phi_i\|s\|c_i\delta_i}{\Phi_i\|s\|+\delta_i} - \sum_{i=1}^{7}\frac{\sigma_i}{\gamma_i}(\tilde{c}_i+c_i)\tilde{c}_i \\
&\leq -s^T(K_m - \frac{\|K_c\|}{2})s - \sum_{i=1}^{7}\frac{\sigma_i}{2\gamma_i}\tilde{c}_i^2 + \frac{\|K_c\|\|x_d\|^2}{2} \\
&\quad + \sum_{i=1}^{7}\frac{\Phi_i\|s\|c_i\delta_i}{\Phi_i\|s\|+\delta_i} + \sum_{i=1}^{7}\frac{\sigma_i}{2\gamma_i}c_i^2 \\
&\leq -\nu V + \kappa
\end{aligned} \tag{23}$$

where $\kappa = \frac{\|K_c\|\|x_d\|^2}{2} + \sum_{i=1}^{7}\frac{\Phi_i\|s\|c_i\delta_i}{\Phi_i\|s\|+\delta_i} + \sum_{i=1}^{7}\frac{\sigma_i}{2\gamma_i}c_i^2$, $\nu = \min(\frac{2\lambda_{min}(K_m-\frac{\|K_c\|}{2})}{\lambda_{max}(\mathcal{M})}, \min_{i=1,2,...7}(\sigma_i))$.

To guarantee $\nu > 0$, the design parameters $K_m - \frac{\|K_c\|}{2} = (K_m - \frac{\|K_c\|}{2})^T > 0$ and $\sigma_i > 0, (i = 1, 2, ...7)$.

Therefore, we can get the equation $\dot{V} \leq -\nu V + \kappa$, which indicates that $s$ converges to a set that containing the origin. Furthermore, the convergence rate could represent as $e^{-\nu t}$.

By integrating both sides of the above equation, we can get the following equation

$$V(t) \leq (V(0) - \frac{\kappa}{\nu})e^{-\nu t} + \frac{\kappa}{\nu} \leq V(0) + \frac{\kappa}{\nu} \tag{24}$$

Thus, for $s$, we have $\frac{1}{2}s^T\mathcal{M}s \leq V(0) + \frac{\kappa}{\nu}$, then we can obtain $\|s\| \leq 2\frac{V(0)+\frac{\kappa}{\nu}}{\lambda_{min}(\mathcal{M})}$. As for $\sum_{i=1}^{7}\frac{1}{2\gamma_i}\tilde{c}_i^2 \leq V(0) + \frac{\kappa}{\nu}$, we could obtain $\max_{i=1,2,...7}(\tilde{c}_i) \leq 2(V(0) + \frac{\kappa}{\nu})(\max_{i=1,2,...7}(\gamma_i))$.

Therefore, the closed-loop signals $s, \tilde{c}_i$ are bounded in the compact set, we can conclude that $V$ is bounded, which indicates that $s \in L_\infty^n$.

ii)From (24), we have $s \in L_\infty^n$. From $s = \dot{e} + \varpi e$, it can be obtained that $e, \dot{e} \in L_\infty^n$. As we have established $e, \dot{e} \in L_\infty^n$, we can have the conclusion that $x(t), \dot{x}(t), \dot{x}_r(t), \ddot{x}_r(t) \in L_\infty^n$, and $\dot{x}(t) \in L_\infty^n$.

As a result, all the signals on the right hand side of (20) are bounded and we can have the conclusion that $\dot{s}$ and $\ddot{x}$ are bounded. Hence, we could obtain that $s \to 0$ as $t \to \infty$. Consequently, $e \to 0$, $\dot{e} \to 0$ as $t \to \infty$. To conclude, $e \to 0$, $\dot{e} \to 0$ as $t \to \infty$.

## VI. Experiments

### A. Control Structure

The powered exoskeleton includes the four-layer control architecture as exoskeleton, distributed embedded system (Elmo driver), servo motor and control unit. From Fig. 5 we can know that the position and angular velocity can be read from the joint sensors and the power signals are generated to activate the actuators. The developed control architecture includes three components: 1) the exoskeleton for sensing and actuation; 2) a motion unit for preforming the lower controller to produce drive force for the exoskeleton joints, nominally running at 1 kHz; 3) a host computer performing a developed application and controlling the graphical display, nominally updating at 100 Hz. The low-level control is realized in real-time by Elmo driver connecting to the computer through CAN bus. The experiment software was developed using Visual C++. The graphical interface shows position sensing signals and tunes controller parameters in experiment trials.

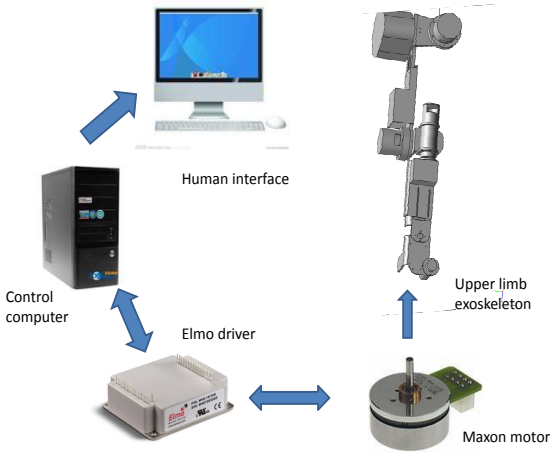


Fig. 5. The control system.

### B. Experimental Setup

To testify the effectiveness of the proposed method, a dual-arm exoskeleton robot is used in this experiment while one arm is worn by human limb as the master and the other arm is performed as the slave. The human controls the trajectories

of the master robot arm and the sEMG signals are acquired from Biceps and Triceps Brachii muscles of the subject and are used to calculate the dynamic stiffness. The master robot arm collects the real-time positions of the human arm and calculates the human arm Jacobian. The experiments are mainly conducted in the presence of the external perturbations which are exerted at the end-point of the slave robot arm.

The purposes of the experiments can be presented as:

(1) When the external perturbations are not exerted at the end-point of the slave robot arm, the slave arm of the exoskeleton robot can follow the trajectory of the master robot arm in synchronization.

(2) If the human limb is in relax state, the slave arm can not reject the existing perturbations which are applied to the end point of the moving slave arm.

(3) In the same situation of (2), the slave arm of the exoskeleton robot is capable of resisting the external perturbations well if the human limb stiffens up.

Four subjects participated in the experiments and they were different in age, height and weight (male, 53kg, 171cm and 24 years old; male, 62kg, 170cm and 26 years old; male, 65kg, 181cm and 22 years old; male, 62kg, 172cm and 25 years old). The perturbations applied at the end-point of the slave robot arm were random and nonlinear according to different subjects. The perturbations were about $12N$ in the experiment of subject 1, about $9N$ in the experiment of subject 2, about $15N$ in the experiment of subject 3, and about $14N$ in the experiment of subject 4.

The external perturbation would be only applied to the end point of the exoskeleton robot in specified periods shown in Table 1. There are four phases in each sub-period and every phase is designed to be 10 seconds. In the first phase, the subject is instructed to keep relax such that the stiffness transferred to the exoskeleton robot is small. In the Cartesian space, the slave robot arm follows the master well in real-time (phase I). In phase II, the perturbation is applied to the slave robot arm. As a contrast to phase II, the operator's limb stiffens up in phase III . Phase IV is the beginning of the other sub-period and it has the same situation of phase I. It should be noted that the master robot arm is always moving during the whole period and the perturbations can be applied to the robot limb in any position in phase II and phase III.

TABLE 1
THE EXPLANATION OF FOUR PHASES IN EXPERIMENT

| | perturbation | limb muscles |
|---|---|---|
| phase I | none | relax |
| phase II | applied | relax |
| phase III | applied | stiffen up |
| phase IV (phase I of the next sub-period) | none | relax |

### C. Experimental Result and Analysis

The experimental results of the control performances of the exoskeleton robot are shown in Figs. 6–12. Fig. 6 shows the reference and actual trajectories of the slave robot arm. Figs. 7 and 8 show the Cartesian errors and the Cartesian stiffness in X/Y direction. Fig. 9 shows the sEMG signals of agonistic/antagonistic muscle pairs. Figs. 10 and 11 present the co-contraction index $a_{cc}$ of the Cartesian stiffness estimation model and the adaptive parameters of the controller. The stiffness ellipsoids are shown in Fig. 12.

In phase I, no external perturbation is exerted to the exoskeleton. When the perturbation is applied to the end point of the slave in phase II, the cartesian errors in X/Y direction increase obviously. The slave can not precisely follow the trajectory of the master robot arm because of the perturbation and the relaxation of the subject's muscles. When the perturbation is removed, the cartesian errors in X/Y direction (7) come back nearly zero quickly. It means that the slave can follow the trajectory of the master robot after the perturbation is removed. It is observed that the transferred stiffness of each direction in cartesian coordinates is small in phase II for the reason that the sEMG signals of human limb is in relax situation.

In contrast to phase II, the muscles of the subject's limb stiffen up in phase III. It can be shown in Fig. 9. The amplitude differences of the transferred stiffness between phase II and phase III in Fig. 8 are obvious. Also, we can see that the values of the co-contraction index $a_{cc}$ in Fig. 10 vary in the same tendency with the sEMG signals. It is observed that the position errors become smaller than that in phase II. Compared phase II with phase III in Figs. 7 and 8, we can see that the proposed impedance transfer skills are effective to reject the external perturbations.

Fig. 11 shows the convergence of the adaptive parameters. At the beginning of the first phase, the 7 parameters are relatively large but tend to decrease and converge to 0. In the second phase, an external disturbance is acted on the slave limb, and the parameters increase rapidly. Then they converge to 0 again. In the third phase, the increase of the parameters is due to the tension of muscles while performing stiffen up in this phase. The adaptive parameters of the controller are able to converge to 0 so as to maintain the stability of the controller. Furthermore, Fig. 12 shows the stiffness ellipsoids which depend on the Cartesian stiffness. The human subject determines the movements and the stiffness which would be transferred to the slave robot arm. The long axis of the ellipse indicates the highest stiffness while the short axis indicates the lowest stiffness.

Subjects 1-4 are different from each other so the movements of their trajectories and errors are various. The ranges of the stiffness in Cartesian space, sEMG signals and the co-contraction indexes $a_{cc}$ are different according to the subjects' self-qualities. Results in Figs. 6–12 suggest that the coordination control is effective for the exoskeleton robot. Based on human impedance transfer skills, the slave robot arm obtains the impedance information calculated from the human's sEMG signals and then uses the coordination control method to track the desired trajectory generated by the master. The proposed controller shows efficiency among different subjects.

## VII. CONCLUSIONS

In this paper, coordination control of a dual-arm exoskeleton robot based on human impedance transfer skills has been pro-

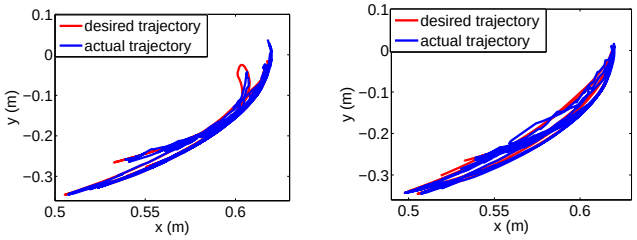


(a) subject 1 (b) subject 2

(c) subject 3 (d) subject 4

Fig. 6. Tracking trajectories in Cartesian Space of 4 subjects

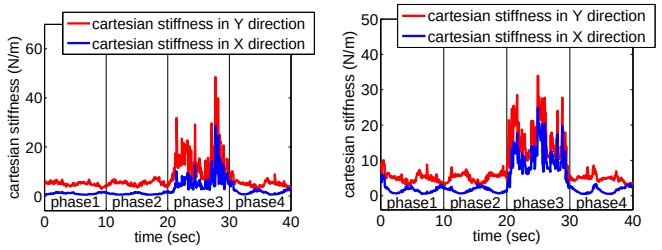


(a) subject 1 (b) subject 2

(c) subject 3 (d) subject 4

Fig. 8. Cartesian stiffness of 4 subjects

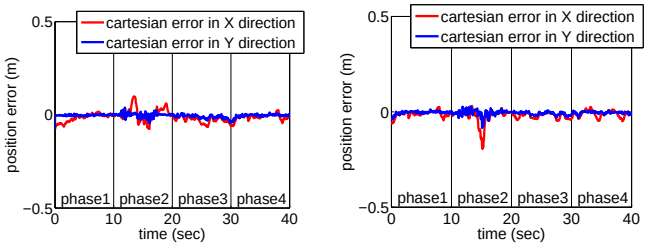


(a) subject 1 (b) subject 2

(c) subject 3 (d) subject 4

Fig. 7. Cartesian errors of 4 subjects

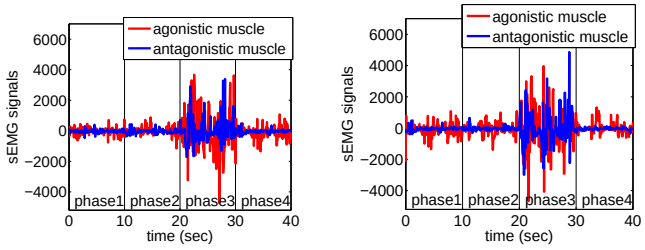


(a) subject 1 (b) subject 2

(c) subject 3 (d) subject 4

Fig. 9. SEMG signals of 4 subjects

posed, where the master arm of the exoskeleton robot extracts the human limb impedance stiffness and position profiles, and then transfers to the slave arm of the exoskeleton. A computationally efficient model of the arm endpoint stiffness behavior is developed and a co-contraction index is defined using muscular activities of a dominant antagonistic muscle pair. A reference command which consists of the stiffness and position information of the operator is computed and realized by the master robot arm in real-time. Considering the dynamics uncertainties of the slave exoskeleton robot performing manipulation, the impedance control incorporating adaptive robust control in the task space has been developed to drive the slave arm of the exoskeleton to track the desired trajectories and make tracking errors convergent. To verify the stableness of the proposed method, an investigation which combines human operation and impedance control under the presence of unknown interactive forces is conducted. By designing the specific experiment and analyzing the experimental results, we demonstrated the efficiency of the proposed technique.

## REFERENCES

[1] Y. Ueyama and E. Miyashita, "Optimal feedback control for predicting dynamic stiffness during arm movement," *IEEE Transactions on Industrial Electronics*, vol. 61, no. 2, pp. 1044-1052, 2014.

[2] Z. Li, B. Wang, F. Sun, C. Yang, Q. Xie, W. Zhang, "sEMG-Based joint force control for an upper-limb power-assist exoskeleton robot," *IEEE Journal of Biomedical and Health Informatics* , vol.18, no. 3, pp. 1043-1050, May 2014.

[3] R. Lu, Z. Li, C.-Y. Su and A. Xue, "Development and learning control of a human limb with a rehabilitation exoskeleton," *IEEE Transactions on Industrial Electronics*, vol. 61, no. 7, pp. 3776-3785, July 2014.

[4] E. Burdet, R. Osu, D. Franklin, T. E. Milner, and M. Kawato, "The central nervous system stabilizes unstable dynamics by learning optimal impedance," *Nature*, vol. 414, no. 6862, pp. 446-449, 2001.

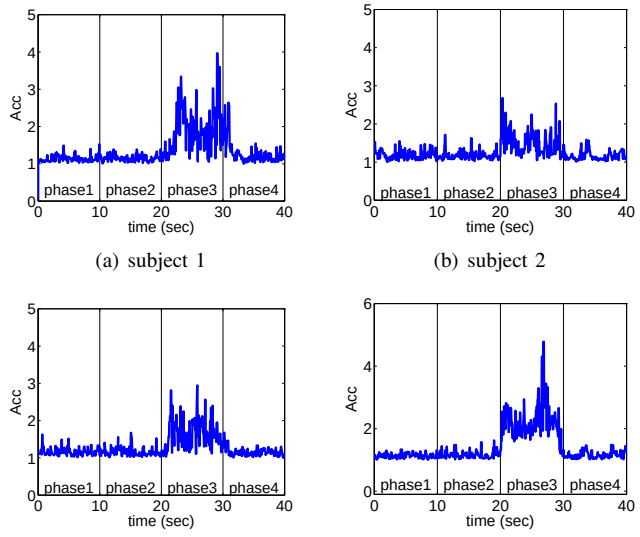


(a) subject 1 (b) subject 2

(c) subject 3 (d) subject 4

Fig. 10. The co-contraction index Acc of 4 subjects

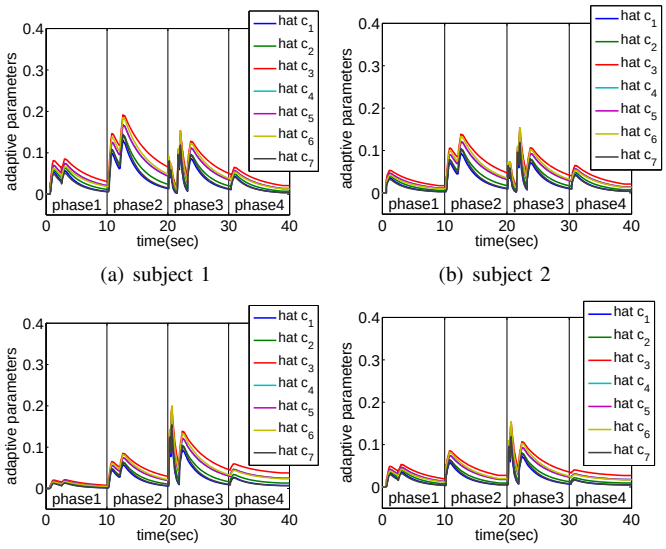


(a) subject 1 (b) subject 2

(c) subject 3 (d) subject 4

Fig. 11. Adaptive parameters of the controller of 4 subjects

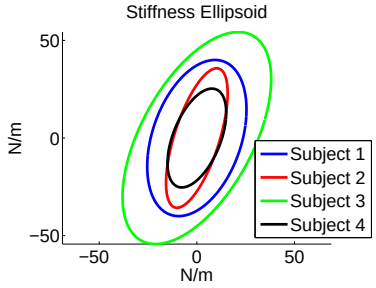


Fig. 12. Stiffness ellipsoids of 4 subjects


[5] A. Ajoudani, N. G. Tsagarakis, and A. Bicchi, "Tele-Impedance: Teleoperation with impedance regulation using a body-machine interface," *International Journal of Robotics Research*, vol. 31, pp. 1642-1655, 2012.

[6] A. Ajoudani, N. Tsagarakis, and A. Bicchi, "Tele-Impedance: Preliminary results on measuring and replicating human arm impedance in tele operated robots," *IEEE International Conference on Robotics and Biomimetics - ROBIO 2011*, pp. 216-223, 2011.

[7] N. Karavas, A. Ajoudani, N. Tsagarakis, J. Saglia, A. Bicchi, and D. Caldwell, "Tele-impedance based assistive control for a compliant knee exoskeleton," *Robotics and Autonomous Systems*, 2014.

[8] A. Ajoudani, S. Godfrey, M. Bianchi, M. Catalano, G. Grioli, N. Tsagarakis, and A. Bicchi, "Exploring teleimpedance and tactile feedback for intuitive control of the Pisa/IIT softhand," *IEEE Transactions on Haptics*, vol. 7, pp. 203-2015, 2014.

[9] J.-S. Hu, J.-J. Wang, and D. M. Ho, "Design of sensing system and anticipative behavior for human following of mobile robots," *IEEE Transactions on Industrial Electronics*, vol. 61, no. 4, pp. 1916-1927, April 2014.

[10] P. L. Gribble, L. I. Mullin, N. Cothros, and A. Mattar, "Role of cocontraction in arm movement accuracy," *Journal of neurophysiology*, vol. 89, no. 5, pp. 2396-2405, 2003.

[11] K. Akazawa, T. Milner, and R. Stein, "Modulation of reflex EMG and stiffness in response to stretch of human finger muscle," *Journal of Neurophisiology*, vol. 49, pp. 16-27, 1983.

[12] R. Trumbower, M. Krutky, B. Yang, and E. Perreault, "Use of selfselected postures to regulate multijoint stiffness during unconstrained tasks," *PLoS One*, vol. 4, no. 5, 2009.

[13] F. Mussa-Ivaldi, N. Hogan, and E. Bizzi, "Neural, mechanical, and geometric factors subserving arm posture in humans," *Journal of Neuroscience*, vol. 5, no. 10, pp. 2732-2743, 1985.

[14] E. Perreault, R. Kirsch, and P. Crago, "Voluntary control of static endpoint stiffness during force regulation tasks," *Journal of Neurophysiology*, vol. 87, pp. 2808-2816, 2002.

[15] D. W. Franklin, E. Burdet, R. Osu, M. Kawato, and T. E. Milner, "Functional significance of stiffness in adaptation of multijoint arm movements to stable and unstable dynamics," *Experimental brain research*, vol. 151, no. 2, pp. 145-157, 2003.

[16] D. Shin, J. Kim, and Y. Koike, "A myokinetic arm model for estimating joint torque and stiffness from emg signals during maintained posture," *Journal of neurophysiology*, vol. 101, no. 1, pp. 387-401, 2009.

[17] R. Osu and H. Gomi, "Multijoint muscle regulation mechanism examined by measured human arm stiffness and EMG signals," *Journal of Neurophysiology*, vol. 81, pp. 1458-1468, 1999.

[18] L. Selen, P. Beek, and J. V. Dieen, "Can co-activation reduce kinematic variability? a simulation study," *Biological Cybernetics*, vol. 93, pp. 373-381, 2005.

[19] M. Kawato, "Internal models for motor control and trajectory planning," *Current opinion in neurobiology*, vol. 9, no. 6, pp. 718-727, 1999.

[20] M. Turvey, "Action and perception at the level of synergies," *Human Movement Science*, vol. 26, no. 4, pp. 657-697, 2007.

[21] T. Milner, "Contribution of geometry and joint stiffness to mechanical stability of the human arm," *Experimental Brain Research*, vol. 143, pp. 515-519, 2002.

[22] A. Ajoudani, C. Fang, N. G. Tsagarakis and A. Bicchi, "A reduced-complexity description of arm endpoint stiffness with applications to teleimpedance control," *IEEE/RSJ International Conference on Intelligent Robots and Systems (IROS), 2015*, pp. 1017-1023, 2015.

[23] M. Chen, S. Ge, "Direct adaptive neural control for a class of uncertain nonaffine nonlinear systems based on disturbance observer," *IEEE Transactions on Cybernetics*, vol. 43, no. 4, pp. 1213-1225, August 2013.

[24] M. Chen, W. Chen, Q. Wu, "Adaptive fuzzy tracking control for a class of uncertain MIMO nonlinear systems using disturbance observer," *SCIENCE CHINA, Information Sciences*. vol. 57, pp. 1-13, January 2014.

[25] D. Ginoya, P. D. Shendge, and S. B. Phadke, "Sliding mode control for mismatched uncertain systems using an extended disturbance observer," *IEEE Transactions on Industrial Electronics*, vol. 61, no. 4, pp. 1983-1992, April 2014.

[26] B. Xu, F. Sun, Y. Pan, "Disturbance observer based composite learning fuzzy control of nonlinear systems with unknown dead zone," *IEEE Transactions on Systems, Man, and Cybernetics: Systems*, DOI: 10.1109/TSMC.2016.2562502, 2016.

[27] S. N. Huang, K. K. Tan, and T. H. Lee, "Adaptive motion control using neural network approximations," *Automatica*, vol. 38, pp. 227C233, 2002.

[28] K. K. Tan, S. N. Huang, and T. H. Lee, "Robust adaptive numerical compensation for friction and force ripple in permanent magnetic linear motors," *IEEE Transactions on Magnetics*, vol. 38, no. 1, pp. 221-228, January 2002.
[29] B. Yao and L. Xu, "Adaptive robust motion control of linear motors for precision manufacturing," *Mechatronics*, vol. 12, pp. 595-616, 2002.
[30] B. Xu, F. Sun, "Composite intelligent learning control of strict-feedback systems with disturbance," *IEEE Transactions on Cybernetics*, DOI: 10.1109/TCYB.2017.
[31] B. Xu, C. Yang, Z. Shi, "Reinforcement learning output feedback NN control using deterministic learning technique," *IEEE Transactions on Neural Networks and Learning Systems*, vol. 25, pp. 635-641, 2014.
[32] Z. Li, H. Xiao, C. Yang, Y. Zhao, "Model predictive control of nonholonomic chained systems using general projection neural networks optimization," *IEEE Transactions onSystems Man and CyberneticsSystems*, vol. 45, no. 10, pp. 1313–1321, Oct. 2015.
[33] Z. Li, S. Xiao, S. S. Ge, and H. Su, "Constrained Multi-legged Robot System Modeling and Fuzzy Control with Uncertain Kinematics and Dynamics Incorporating Foot Force Optimization," *IEEE Transactions on Systems Man and Cybernetics: Systems*, vol. 46, no. 1, pp. 1–15, 2016.
[34] S. Calinon, P. Evrard, E. Gribovskaya, A. Billard, and A. Kheddar, "Learning collaborative manipulation tasks by demonstration using a haptic interface," *International Conference on Advanced Robotics*, 2009.
[35] E. Gribovskaya, K. Abderrahmane, B. Aude, "Motion learning and adaptive impedance for robot control during physical interaction with humans," *Robotics and Automation (ICRA), 2011 IEEE International Conference on Robotics and Automation*, pp. 4326-4332, 2011.
[36] N. Sornkarn, T. Nanayakkara, "Can a soft robotic probe use stiffness control like a human finger to improve efficacy of haptic perception," *IEEE Transactions on Haptics*, pp. 1939-1412, 2016.
[37] J. K. Salisbury, "Active stiffness control of a manipulator in Cartesian coordinates," *Proceedings of the 19th IEEE Conference on Decision and Control*, pp. 87-97, 1980.
[38] I. Kao and C. Ngo, "Properties of the grasp stiffness matrix and conservative control strategies," *The International Journal of Robotics Research*, vol. 18, no. 2, pp. 159-167, 1999.
[39] C. E. Clauser, J. T. McConville, and J. W. Young, "Weight, volume, and center of mass of segments of the human body," *DTIC Document, Tech. Rep.*, 1969.
[40] E. Perreault, R. Kirsch, and R. Crago, "Multijoint dynamics and postural stability of the human arm," *Experimental Brain Research* pp. 507-517, 2004.
[41] C. Chen and W. Chang, "A feedforward neural network with function shape autotuning," *Neural networks*, vol. 9, no. 4, pp. 627-641, 1996.
[42] S. S. Ge, T. H. Lee, and C. J. Harris, "Adaptive neural network control of robot manipulators," *World Scientific*, London, 1998.
[43] Z. Li, S. S. Ge, Z. Wang, "Robust adaptive control of coordinated multiple mobile manipulators," *Mechatronics*, vol. 18, pp. 239-250, 2008.